EUROPEAN ORGANIZATION FOR NUCLEAR RESEARCH

CERN-PPE/92-219
17 December 1992

STUDY OF THE CENTRALLY PRODUCED $\omega\rho^0$ AND $\omega\omega$ SYSTEMS IN pp INTERACTIONS AT 300 GeV/c

WA76 Collaboration
Athens–Bari–Birmingham–CERN–Collège de France

T.A. Armstrong[4,a)], M. Benayoun[5)], I.J. Bloodworth[3)], J.N. Carney[3)], C. Evangelista[2)], B.R. French[4)], B. Ghidini[2)], M. Girone[2)], A. Jacholkowski[2)], J. Kahane[5)], J.B. Kinson[3)], A. Kirk[4)], K. Knudson[4)], V. Lenti[2)], Ph. Leruste[5)], A. Malamant[5)], J.L. Narjoux[5)], F. Navach[2)], A. Palano[2)], N. Redaelli[4,b)], L. Rossi[4,c)], M. Sené[5)], R. Sené[5)], M. Stassinaki[1)], G. Vassiliadis[1)], O. Villalobos Baillie[3)], M.F. Votruba[3)] and G. Zito[2)]

Abstract

We have performed a search for vector–vector final states centrally produced in proton proton interactions at 300 GeV/c using the CERN Ω spectrometer. Evidence is found for $\omega\rho^0$ production in the reaction $pp \to p_f(2\pi^+2\pi^-\pi^0)p_s$ and for $\omega\omega$ production in the reaction $pp \to p_f(2\pi^+2\pi^-2\pi^0)p_s$. However no evidence is found for $\omega\phi$ production in the reaction $pp \to p_f(K^+K^-\pi^+\pi^-\pi^0)p_s$.

Submitted to Zeitschrift für Physik C

1) Athens University, Nuclear Physics Department, Athens, Greece
2) Dipartimento di Fisica dell'Università and Sezione INFN, Bari, Italy
3) University of Birmingham, Physics Department, Birmingham, U.K.
4) CERN, European Organization for Nuclear Research, Geneva, Switzerland
5) Collège de France, Paris, France
a) Present address: Pennsylvania State University, University Park, USA
b) Present address: INFN and Dipartimento di Fisica, Milan, Italy
c) Present address: INFN and Dipartimento di Fisica, Genoa, Italy

1 Introduction

The search for non $q\bar{q}$ mesons such as glueballs, hybrids and multiquark states is the main motivation of present hadron spectroscopy. Searches for new resonances decaying to two vector mesons have been performed extensively in hadron induced reactions [1] [2], $\gamma\gamma$ collisions [3] and J/ψ radiative decays [4].

The study of associated $\phi\phi$ production in π^-p interactions [5] was one of the starting points of gluonium spectroscopy. The large and unexpected $\phi\phi$ cross section in π^- p interactions has been interpreted as due to the production of three $J^{PC} = 2^{++}$ glueball states in the 2.0 - 2.5 GeV region.

Evidence for resonant structures in the 1.6 and 2.0 GeV regions has been recently reported in the $\omega\omega$ system produced by incident π^- [2]. The study of $K^*\bar{K}^*$ and $\phi\phi$ from K^- induced reactions, on the other hand, did not show any evidence for resonance production [1].

As regards the J/ψ radiative decays, the $\phi\phi$, $\omega\omega$, $K^{*0}\bar{K}^{*0}$ and $\rho\rho$ final states are dominated by $J^P = 0^-$ contributions. These spectra show marked threshold enhancements, whereas the $\rho\rho$ final state shows the presence of resonant structures.

Associated vector-vector production in $\gamma\gamma$ collisions has provided evidence for an unexpected $\rho^0\rho^0$ threshold enhancement not observed in the $\rho^+\rho^-$ final state. This observation has been interpreted as due to the presence of new exotic 4-quark resonances.

Another interesting candidate for a multiquark state comes from $p\bar{p}$ annihilation at rest to 3π which led to the discovery of a $J^{PC} = 2^{++}$ resonance decaying to $\pi\pi$ ($f_2(1520)$) [6].

A molecular hypothesis has also been made [7] to explain the nature of the $\theta(1720)$ discovered in J/ψ decay and clearly observed in central hadronic collisions by WA76 experiment [8]. This hypothesis predicts $K^{*0}\bar{K}^{*0}$ and $\phi\omega$ decays for the $\theta(1720)$.

The WA76 experiment, at the CERN Ω spectrometer, has performed a systematic exploration of resonance production in the central region of hadronic collisions [9]. The search for vector–vector final states has provided evidence for centrally produced $\phi\phi$ [10] and $K^{*0}\bar{K}^{*0}$ [11]. It is therefore of interest to study other vector–vector final states which could give new information and help in the understanding of the dynamics underlying the production of resonances in this kinematical region.

Details on the layout of the apparatus of the WA76 experiment, trigger conditions and data processing have been given in a previous publication [12]. This paper describes the search for final states involving the $\omega(783)$ meson, i.e. $\omega\rho^0$, $\omega\phi$ and $\omega\omega$, in the reactions:

$$pp \rightarrow p_f(\omega V)p_s$$

at 300 GeV/c, where the subscripts f and s indicate the fastest and the slowest particles in the laboratory respectively and V is a vector meson.

This paper is organized as follows. In section 2 we describe the study of the $2\pi^+2\pi^-\pi^0$ final state and the evidence for $\omega\rho^0$ production. Section 3 is devoted to the search for $\omega\phi$ by

studying the $K^+K^-\pi^+\pi^-\pi^0$ final state and section 4 shows evidence for the $\omega\omega$ system in the $2\pi^+2\pi^-2\pi^0$ final state. Finally section 5 summarizes the results from this analysis.

2 Study of the $2\pi^+2\pi^-\pi^0$ channel

The reaction

$$pp \to p_f(2\pi^+2\pi^-\pi^0)p_s \tag{1}$$

has been selected from the sample of events having six outgoing charged tracks and only two γ's having an energy greater than 1.0 GeV deposited in the electromagnetic calorimeters [13], by first imposing the following cuts on the components of missing momentum: |missing P_x| < 20.0 GeV/c, |missing P_y| < 0.16 GeV/c, |missing P_z| < 0.08 GeV/c, where the x axis is along the beam direction. Showers associated with charged track impacts on the electromagnetic calorimeters have been removed.

The effective mass distribution of the two γ's is shown in fig. 1, where a clear π^0 signal can be seen. After selecting the π^0 events by requiring $0.096 \leq m(\gamma\gamma) \leq 0.174$ GeV, the energies of the γ's have been recomputed in order to give the π^0 mass. The central charged particles were then required, if passing through the Cerenkov system, to have a mass identification consistent with that of the pion. Events where the slow particle was identified as a π^+ were antiselected using pulse height momentum correlation. The energy balance was required by demanding the function Δ, defined as:

$$\Delta = MM^2(p_f p_s) - M^2(2\pi^+2\pi^-\pi^0)$$

to be in the range from –5.0 to 5.0 GeV^2. Only π^0's with a centre of mass rapidity less than 1.9 were retained in order to remove π^0's from diffractive processes. A similar cut was also used to antiselect diffractive π^+'s. The final sample consists of about 8000 events.

Fig. 2 shows the Feynman x_F distributions for the protons and the $2\pi^+2\pi^-\pi^0$ system after having applied the cuts described above. We observe that the central system is well separated from the fast and the slow particles. The $2\pi^+2\pi^-\pi^0$ effective mass distribution is shown in fig. 3: enhancements can be seen at the η' and $f_1(1285)$ positions. Fig. 4 shows the combinatorial $\pi^+\pi^-\pi^0$ mass spectrum (4 entries per event), where clear η and $\omega(783)$ signals can be observed, which are due to the presence of the reactions:

$$pp \to p_f(\eta\pi^+\pi^-)p_s \tag{2}$$

$$pp \to p_f(\omega\pi^+\pi^-)p_s \tag{3}$$

The $\eta\pi^+\pi^-$ system in reaction (2) has been studied in a previous paper [14] and is dominated by the presence of η' and $f_1(1285)$ mesons.

2.1 Study of the $\omega\pi^+\pi^-$ system

We have performed a study of reaction (3) by first trying to solve the combinatorial problem which affects the $\omega(783)$ signal. Since the $\omega(783)$ is a $J^P = 1^-$ state it is useful to introduce the parameter λ which describes the ω decay on the Dalitz plot, defined as:

$$\lambda = \frac{|\vec{p}_+ \times \vec{p}_-|^2}{\frac{3}{4}(\frac{1}{9}m^2 - m_\pi^2)^2}$$

where $|\vec{p}_+ \times \vec{p}_-|$ is proportional to the decay matrix element of $\omega \to \pi^+\pi^-\pi^0$, $\vec{p}_\pm$ is the three momentum of the $\pi^\pm$ in the ω rest frame and m^2 is the $\pi^+\pi^-\pi^0$ squared effective mass.

Fig. 4 (hatched histogram) shows the $\pi^+\pi^-\pi^0$ effective mass distributions for events having $\lambda \leq 0.3$ where little $\omega(783)$ can be seen. Thus this cut removes part of the background with little reduction of the $\omega(783)$ signal.

Fig. 5a) shows the $\pi^+\pi^-$ vs $\pi^+\pi^-\pi^0$ scatter plot for events having $\lambda > 0.3$. The $\pi^+\pi^-$ effective mass distributions in the $\omega(783)$ region ($0.74 \leq m(\pi^+\pi^-\pi^0) \leq 0.84$ GeV) and in its side bands ($0.69 \leq m(\pi^+\pi^-\pi^0) \leq 0.74$ GeV and $0.84 \leq m(\pi^+\pi^-\pi^0) \leq 0.89$ GeV) are shown in figs 5b) and 5c) respectively. A $\rho^0(770)$ can be seen in the $\pi^+\pi^-$ mass spectrum associated with the $\omega(783)$, but no signal is observed in the wings, indicating evidence for the production of the $\omega\rho^0$ final state.

2.2 Channel likelihood fit of the $\omega\pi^+\pi^-$ system

In order to extract the mass spectra free from the combinatorial background and to determine the different reactions that may contribute to the observed final states a channel likelihood fit [15], has been performed using a modified version of the program CHAFIT [16]. The program performs a maximum likelihood fit of different overlapping amplitudes and gives to each event a probability that it belongs to one of the input hypotheses. The amplitudes used in the fit were Breit-Wigner formulae fixed to the PDG [17] values to describe the $\rho(770)$ and the $b_1(1235)$. The η and $\omega(783)$ have been described as Gaussians for which m_0 and σ have been obtained by fitting the $\pi^+\pi^-\pi^0$ effective mass distribution ($m_\eta = 0.549$, $\sigma_\eta = 0.011$, $m_\omega = 0.783$, $\sigma_\omega = 0.018$ GeV). In addition, the $\omega(783)$ amplitude has been multiplied by the parameter λ described above, including in this way the information coming from the spin-parity of this state. All the amplitudes have been normalized using Monte-Carlo events obtained by event mixing.

The results of the fit performed to the total $2\pi^+2\pi^-\pi^0$ mass spectrum are shown in table 1. The main results can be summarized as follows.

- The final states involving the production of ρ^+, ρ^0, ρ^- are produced approximately with the same intensity. There is evidence for associated production of $\rho^0\rho^\pm\pi^\mp$ but the $\rho^0\rho^\pm\pi^\mp$ effective mass distribution (not shown) does not show evidence for a resonant behaviour.

- No evidence is found for $\rho^0\rho^0\pi^0$ production.
- There is small but significant $\omega\rho^0$ production ($3.8 \pm 0.6\%$ corresponding to 304 ± 50 events).

We have then used the following method in order to extract the sample of events belonging to reaction (3). From the channel likelihood fit we obtain a probability to each of the four possible combinations of the $\pi^+\pi^-\pi^0$ to belong to the $\omega(783)$. Therefore, in order to solve the combinatorial problem we have considered the ω combination having the highest probability. In addition, we required this probability to be greater then 0.35. This cut leaves no ω signal in the excluded data, obtaining in this way a sample of events free from combinatorials, which are candidates for the $\omega\pi^+\pi^-$ channel. The resulting $\omega\pi^+\pi^-$ mass spectrum is shown in fig. 6a). The $\omega\pi^\pm$ mass distribution (fig. 6b)) shows the signal of the $b_1^\pm(1235)$ meson. Selecting events in the range $1.16 \leq m(\omega\pi) \leq 1.32$ GeV we obtain the $b_1^\pm(1235)\pi^\mp$ mass spectrum shown in fig. 6c), where no significant resonant structure can be seen.

The $\pi^+\pi^-$ effective mass distribution is shown in fig. 6d), where we observe a peak at the $\rho^0(770)$ position. The $\omega\rho^0$ mass distribution shown in fig. 6e) is obtained by requiring $0.68 \leq m(\pi^+\pi^-) \leq 0.88$ GeV, to select the $\rho^0(770)$ signal.

A spin-parity analysis of the $\omega\rho^0$ system has been performed using Zemach tensors. The decay matrix elements for a state X which decays to $\omega\pi^+\pi^-$ through the decay chain $X \to \omega\rho^0 \to \omega\pi^+\pi^-$, with an orbital momentum L between the $(\pi^+\pi^-)$ system and the $\omega(783)$ limited to values smaller than 2 are given in table 2. Due to the limited statistics we were only able to search for the dominant spin-parity wave. For this purpose the different spin amplitudes have been inserted in different combinations in the channel likelihood fit. If we assume that one wave dominates the spectrum we find the best description of the data is obtained with $J^P = 2^-$. Some information on the angular analysis is shown in fig. 7a,b) where we have plotted the combinatorial distribution of the angle χ which is defined as the azimuthal angle between the normal to the ω and the direction of the π^+ of the ρ^0 in the $\omega\rho^0$ rest frame. Here the crosses show the data while the broken lines represent the expectations for different spin-parity combinations. The geometrical acceptance does not affect the angular distributions. We notice that the best description of the data is given by the spin 2 amplitudes which are very similar when plotted as a function of χ.

3 Study of the $K^+K^-\pi^+\pi^-\pi^0$ channel

The reaction:

$$pp \to p_f(K^+K^-\pi^+\pi^-\pi^0)p_s \tag{4}$$

has been selected from the sample of six prongs events having two γ's detected in the electromagnetic calorimeters, each with an energy greater then 1.0 GeV by first requiring momentum balance as described in section 2. Moreover one of the central charged particles was required to be positively identified as a K or ambiguous K/p, the second to have a mass assignment compatible with the kaon hypothesis, while the remaining two particles

were required to have a mass assignement compatible with that of the pion, as given by the Cerenkov information. The energy balance was then ensured by requiring the Ehrlich mass squared, computed as a function of the two kaon candidates [18] and shown in fig. 8a), to be in the range: $0.12 \leq m_X^2 \leq 0.56$ GeV^2. The three enhancements visible in fig. 8a) are the signals of the centrally produced $2\pi^+2\pi^-\pi^0$ (due to the inefficiency of the Cerenkov identification), $K^+K^-\pi^+\pi^-\pi^0$ and $p\bar{p}\pi^+\pi^-\pi^0$ final states respectively. Forward $\Delta^+ \rightarrow p_f\pi^0$ has been removed by requiring the centre of mass rapidity of the π^0 to be smaller than 2.0.

The final sample consists of 662 events. The $K^+K^-\pi^+\pi^-\pi^0$ mass spectrum is shown in fig. 8b) which shows no evidence for any structure. Fig. 9a) shows the scatter plot $m(\pi^+\pi^-\pi^0)$ vs $m(K^+K^-)$ where no accumulation of events is visible in the region where the ω and ϕ bands overlap. We also observe that the $m(K^+K^-)$ projection, fig. 9b), shows little signal in the region of the $\phi(1020)$ meson, as does the corresponding $m(pi^+pi^-pi^0)$ projection, fig. 9c) in the $\omega(783)$ region. Therefore we conclude that there is no evidence, with the present statistics, for associated $\omega\phi$ production.

We have also searched, in reaction (4), for the $K^{*0}\bar{K}^{*0}\pi^0$ final state. Fig. 10a) shows the $K^+\pi^-$ vs $K^-\pi^+$ scatter plot where little accumulation of events can be seen in the region of the overlapping K^{*0} bands. The $K^\pm\pi^\mp$ mass distribution is shown in fig. 10b) where a clear K^{*0} signal can be seen. In order to search for the $K^{*0}\bar{K}^{*0}\pi^0$ final state, table 3 shows the event distribution on the $K^-\pi^+$ vs $K^+\pi^-$ scatter plot of fig 10a) in 9 bins centred around the K^{*0} mass. The resulting number of events of associated $K^{*0}\bar{K}^{*0}$ production, taking into account the K^* Breit-Wigner tails, is of 30 ± 10 events. We conclude therefore that there is also little evidence for the $K^{*0}\bar{K}^{*0}\pi^0$ final state.

4 Study of the $2\pi^+2\pi^-2\pi^0$ channel

The reaction:

$$pp \rightarrow p_f(2\pi^+2\pi^-2\pi^0)p_s \tag{5}$$

has been selected from the sample of events having six outgoing charged tracks and only four γ's detected in the electromagnetic calorimeters. Momentum balance was ensured by requiring |missing P_x| < 20.0 GeV/c, |missing P_y| < 0.36 GeV/c and |missing P_z| < 0.18 GeV/c. The energy balance was obtained by demanding the function Δ, defined as:

$$\Delta = MM^2(p_f p_s) - M^2(2\pi^+2\pi^-2\pi^0)$$

to be $|\Delta| \leq 6.0$ GeV^2.

Fig. 11a) shows the $\gamma_1\gamma_2$ vs $\gamma_3\gamma_4$ "lego" plot showing evidence for $\pi^0\pi^0$ production. Selecting one π^0 in the region $0.10 \leq m(\gamma\gamma) \leq 0.17$ GeV we obtain the $\gamma\gamma$ effective mass distribution shown in fig. 11b).

In order to search for $\omega\omega$ production which is affected by a combinatorial background we have applied to each $\pi^+\pi^-\pi^0$ combination the cut $\lambda > 0.3$, where the parameter λ has been described in section 2. Fig. 12a) shows the scatter plot $\pi^+\pi^-\pi^0$ vs. $\pi^+\pi^-\pi^0$ (4

entries per event) where an accumulation of events can be observed at the position of the $\omega\omega$ production. Fig. 12b) shows the combinatorial $\pi^+\pi^-\pi^0$ effective mass where a clear $\omega(783)$ signal can be seen. Requiring one $\pi^+\pi^-\pi^0$ combination to be in the $\omega(783)$ region ($0.742 \leq m(\pi^+\pi^-\pi^0) \leq 0.822$ GeV) we obtain the $\pi^+\pi^-\pi^0$ mass spectrum shown in fig. 12c), where the $\omega(783)$ signal can be clearly seen with little background. The $\omega\omega$ mass distribution shown in fig. 13a) is obtained by selecting events giving combinations with two $\pi^+\pi^-\pi^0$ assignments in the $\omega(783)$ region, and giving these the ω mass.

An analysis of the angular distributions has been performed in order to estimate whether the $\omega\omega$ production belongs to states with definite spin-parity. We have plotted, in fig. 13b,c), the distribution of χ, the azimuthal angle between the normals to the two decay planes of the ω's in the $\omega\omega$ rest frame. These distributions have been corrected for geometrical acceptance which is, however, nearly flat as a function of χ. The distribution is expected to follow the formula [19]

$$\frac{dN}{d\chi} = 1 + \beta cos2\chi$$

where β = -1, 2/3 and 1/15 for $J^P = 0^-, 0^+$ and 2^+ (in the lowest angular momentum between the two ω) respectively. The distributions in fig. 13a,b) have been obtained selecting two $\omega\omega$ regions: (m < 1.8 GeV) and (1.8 < m < 2.08 GeV). It can be seen that the 0^- is less favoured than 0^+ or 2^+.

5 Conclusions

In conclusion, we have performed a search for centrally produced vector–vector final states in proton proton interactions at 300 GeV/c using the CERN Ω spectrometer. Evidence is found for $\omega\rho^0$ production in the reaction $pp \to p_f(2\pi^+2\pi^-\pi^0)p_s$ and $\omega\omega$ production in the reaction $pp \to p_f(2\pi^+2\pi^-2\pi^0)p_s$. No evidence is found for $\omega\phi$ production in the reaction $pp \to p_f(K^+K^-\pi^+\pi^-\pi^0)p_s$.

REFERENCES

[1] D. Aston et al. Nucl. Phys. B21 (Proc. Suppl.) (1991) 5.

[2] D. Alde et al. Phys. Lett. B205 (1988) 451;
D. Alde at al., Phys. Lett. B241 (1990) 600;
G.M. Beladidze et al., Z. Phys. C54 (1992) 367.

[3] S. Kawabata. Proceedings of the Joint International Lepton-Photon Symposium & Europhysics Conference on High Energy Physics, LP-HEP 91, Geneva, Switzerland, 25 July - 1 August 1991.

[4] G. Eigen. Proceedings of the IIIrd International Conference on Hadron Spectroscopy, Hadron '89, Ajaccio, Corsica, France. September 23-27, 1989.

[5] A. Etkin et al., Phys. Lett. 201B (1988) 568.

[6] B. May et al., Phys. Lett. 225B (1989) 450;
E. Aker et al., Phys. Lett. 260B (1991) 249.

[7] K. Dooley et al., Phys. Lett. 275B (1992) 478.

[8] T.A. Armstrong et al., Phys. Lett. 227B (1989) 186.

[9] A. Palano, Resonance production in central hadronic collision, CERN/PPE 92-93, 18 May 1992.

[10] T.A. Armstrong et al., Phys. Lett. B146 (1984) 273;
T.A. Armstrong et al., Phys. Lett. B221 (1989) 221.

[11] T.A. Armstrong et al., Z. Phys. C35 (1987) 167;
T.A. Armstrong et al., Z. Phys. C46 (1990) 405;

[12] T.A. Armstrong et al., Nucl. Instr. and Meth. A276 (1989) 165.

[13] H. Burmeister et al., Nucl. Instr. and Meth. A225 (1984) 530;
M. Bonesini et al., Nucl. Instr. and Meth. A261 (1987) 471.

[14] T.A. Armstrong et al., Z. Phys. C52 (1991) 389.

[15] P.E. Condon and P. Cowell, Phys. Rev. D9 (1974) 2268.

[16] Ph. Gavillet and J.C. Marin, CHAFIT, CERN/D.Ph.II/PROG 75-2 (1975).

[17] Review of Particle Properties. Phys. Rev D45 (1992).

[18] R. Ehrlich et al., Phys. Rev. Lett. 20 (1968) 686;
T. Armstrong et al., Z. Phys. C51 (1991) 351.

[19] N.P Chang and C.T. Nelson, Phys. Rev. Lett. 40 (1978) 1617;
T.L. Trueman, Phys. Rev. D18 (1978) 3423.

TABLE CAPTIONS

Tab. 1 : Results from the Channel likelihood fit.

Tab. 2 : Decay matrix elements for $X \to \omega\rho^0$.

Tab. 3 : Event distribution on the $K^-\pi^+$ vs $K^+\pi^-$ scatter plot centered around the $K^{*0}\bar{K}^{*0}$ position.

Table 1:

Channel	Percentage
$p_f(\rho^0\pi^+\pi^-\pi^0)p_s$	10.4 ± 2.4
$p_f(\rho^+\pi^-\pi^+\pi^-)p_s$	8.2 ± 1.5
$p_f(\rho^-\pi^+\pi^+\pi^-)p_s$	14.1 ± 1.5
$p_f(\eta\pi^+\pi^-)p_s$	4.1 ± 0.3
$p_f(\omega\pi^+\pi^-)p_s$	12.2 ± 1.1
$p_f(\omega\rho^0)p_s$	3.8 ± 0.6
$p_f(b_1^{\pm}(1235)\pi^{\mp})p_s$	2.9 ± 0.8
$p_f(\rho^0\rho^{\pm}\pi^{\mp})p_s$	15.4 ± 2.0
phase space	28.8 ± 2.8

Table 2:

L	J^P	Matrix element
0	0^+	$\vec{n} \cdot \vec{\pi}$
0	1^+	$\vec{n} \times \vec{\pi}$
0	2^+	$a_{ij}(\vec{n}, \vec{\pi})$
1	0^-	$\vec{n} \cdot (\vec{\omega} \times \vec{\pi})$
1	1^-	$\vec{n} \times (\vec{\omega} \times \vec{\pi})$
1	2^-	$a_{ij}(\vec{n}, \vec{\omega} \times \vec{\pi})$

The symbols used in this table have the following meaning:
$a_{ij}(\vec{v}, \vec{w}) = \frac{1}{2}(v_i w_j + v_j w_i) - \frac{1}{3}\delta_{ij}(v \cdot w)$
$\vec{n}$: normal to the decay plane of the ω
$\vec{\omega}$: three-momentum of the ω, in the total rest frame
$\vec{\pi}$: three-momentum of one π, in the $\pi^+\pi^-$ rest frame

Table 3:

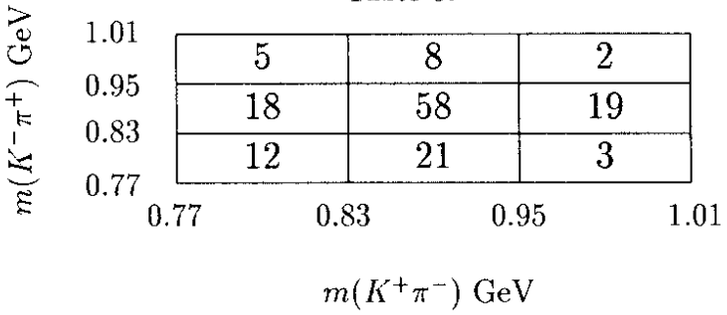

FIGURE CAPTIONS

Fig. 1 : $\gamma\gamma$ effective mass distribution for event candidates to reaction (1) which balance momentum.

Fig. 2 : Feynman x_F distribution for the slow proton, the $2\pi^+2\pi^-\pi^0$ system and the fast proton.

Fig. 3 : $2\pi^+2\pi^-\pi^0$ effective mass distribution for reaction (1).

Fig. 4 : Combinatorial $\pi^+\pi^-\pi^0$ effective mass distribution (4 entries per event)from reaction (1). The hatched histogram represents the events antiselected by requiring $\lambda < 0.3$ (see text).

Fig. 5 : a) Combinatorial scatter plot $\pi^+\pi^-$ vs. $\pi^+\pi^-\pi^0$ from reaction (1) requiring $\lambda > 0.3$;
b) $\pi^+\pi^-$ effective mass distribution opposite to the ω;
c) $\pi^+\pi^-$ effective mass distribution in the side bands of the ω.

Fig. 6 : Effective mass distributions obtained by using the results of the channel likelihood fit (see text).

Fig. 7 : Angular distributions of the $\omega\rho^0$ system (see text). The crosses represent the data, the broken lines the expectations for various spin-parity assignments, a) for positive parity states, b) for negative parity states.

Fig. 8 : a) Ehrlich mass distribution for event candidates to reaction (4);
b) $K^+K^-\pi^+\pi^-\pi^0$ effective mass distribution.

Fig. 9 : a) $\pi^+\pi^-\pi^0$ vs. K^+K^- scatter plot from reaction (4);
b) K^+K^- effective mass distribution;
c) $\pi^+\pi^-\pi^0$ effective mass distribution.

Fig. 10 : a) $K^-\pi^+$ vs. $K^+\pi^-$ scatter plot from reaction (4);
b) $K\pi$ effective mass distribution.

Fig. 11 : a) $\gamma\gamma$ vs. $\gamma\gamma$ lego plot for event candidates to reaction (5) and balancing momentum;
b) $\gamma\gamma$ effective mass distribution after having required the associated γ's pair to come from a π^0 decay.

Fig. 12 : a) Combinatorial $\pi^+\pi^-\pi^0$ vs. $\pi^+\pi^-\pi^0$ scatter plot from reaction (5). A cut $\lambda > 0.3$ is applied to both combinations;
b) Combinatorial $\pi^+\pi^-\pi^0$ effective mass with $\lambda > 0.3$;
c) $\pi^+\pi^-\pi^0$ effective mass distribution associated with an ω after having required $\lambda > 0.3$ to both combinations.

Fig. 13 : a) $\omega\omega$ effective mass distribution;
b,c) $\omega\omega$ angular distributions (see text). The crosses represent the data. The superimposed curves are expectations for: $J^P = 2^+$ (solid), 0^- (dashed), 0^+ (dotted) respectively.

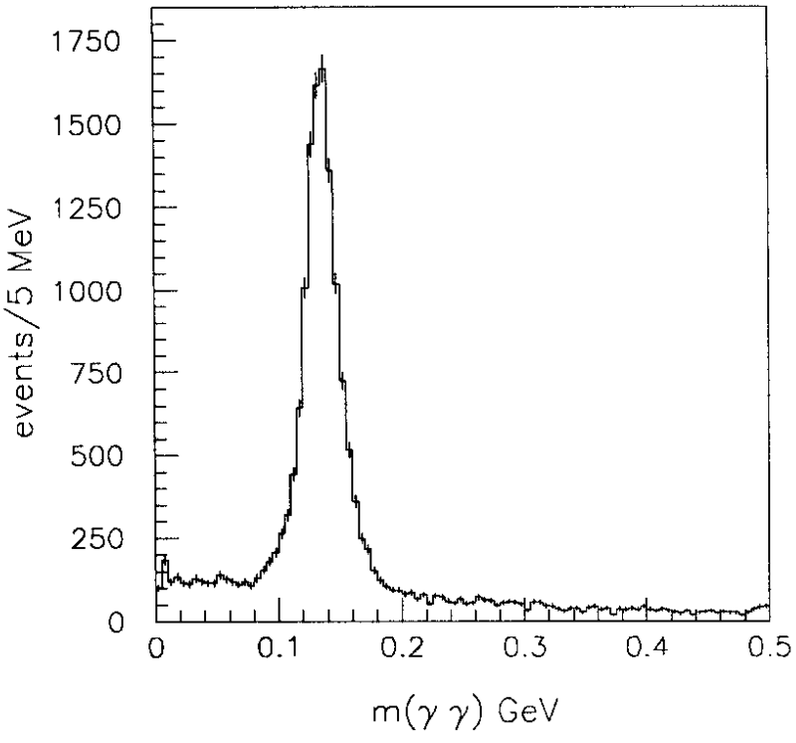
1750
1500
1250
1000
750
500
250
0
events/5 MeV
0
0.1
0.2
0.3
0.4
0.5
m(γ γ) GeV

Fig. 1

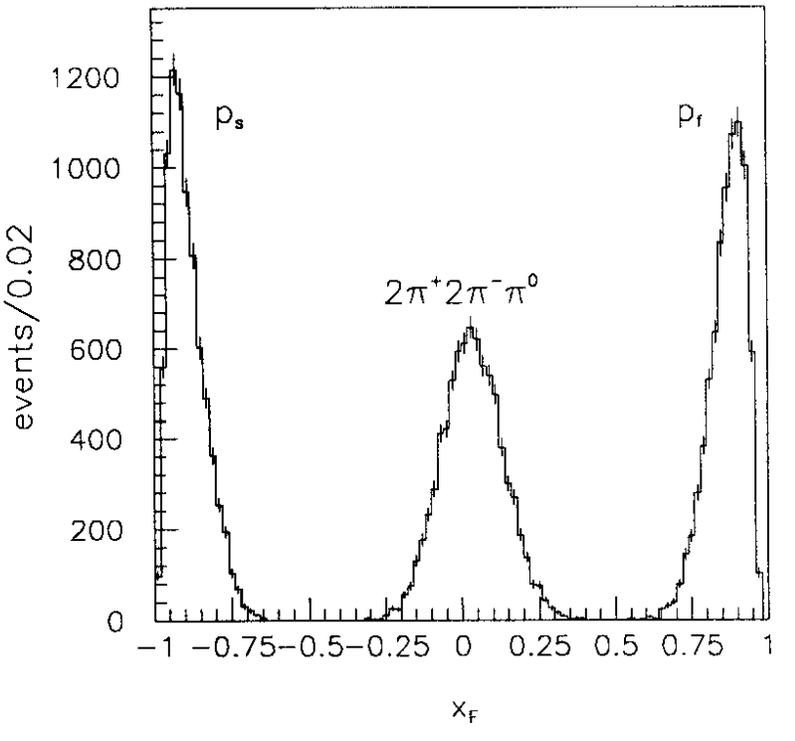
1200
1000
800
600
400
200
0
events/0.02
p_s
p_f
2π⁺2π⁻π⁰
−1
−0.75
−0.5
−0.25
0
0.25
0.5
0.75
1
x_F

Fig. 2

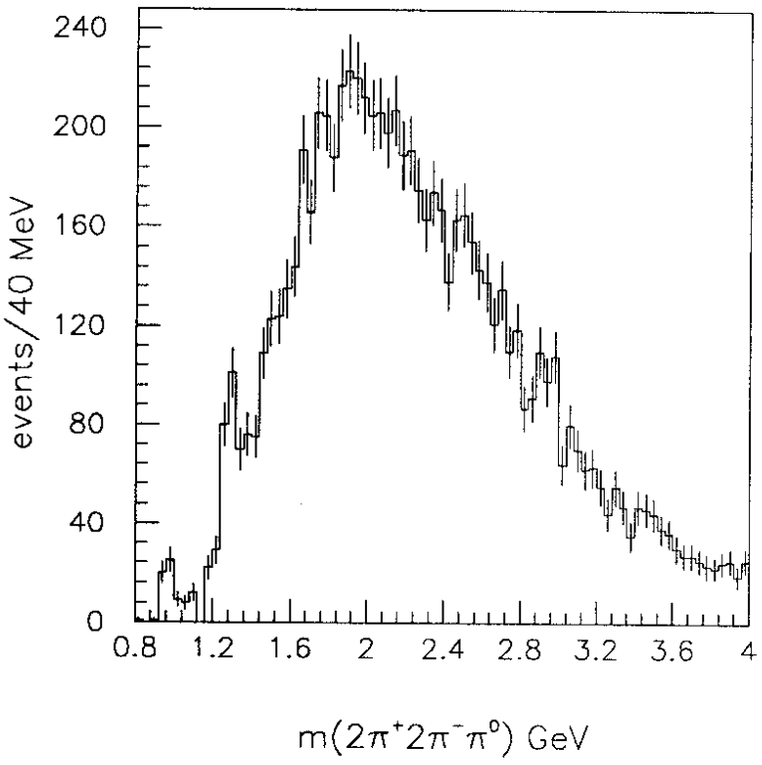
240
200
160
120
80
40
0
events/40 MeV
0.8
1.2
1.6
2
2.4
2.8
3.2
3.6
4
m(2π⁺2π⁻π⁰) GeV

Fig. 3

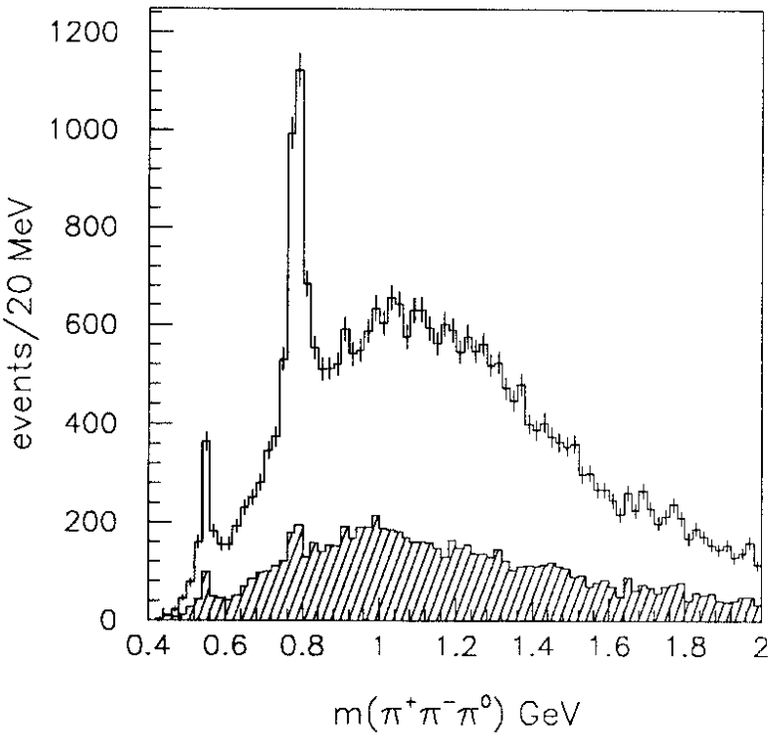
1200
1000
800
600
400
200
0
events/20 MeV
0.4
0.6
0.8
1
1.2
1.4
1.6
1.8
2
m(π⁺π⁻π⁰) GeV

Fig. 4

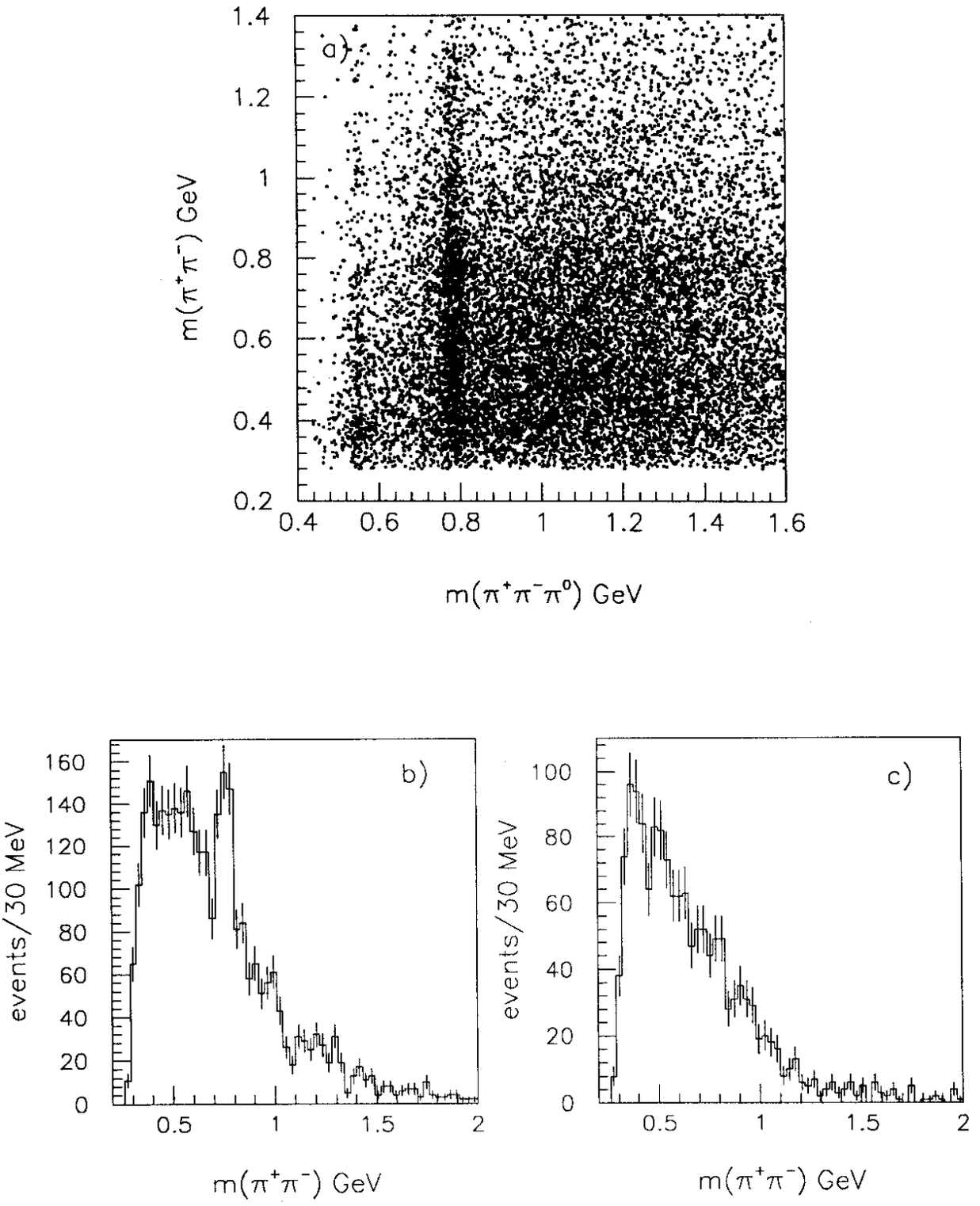

Fig. 5

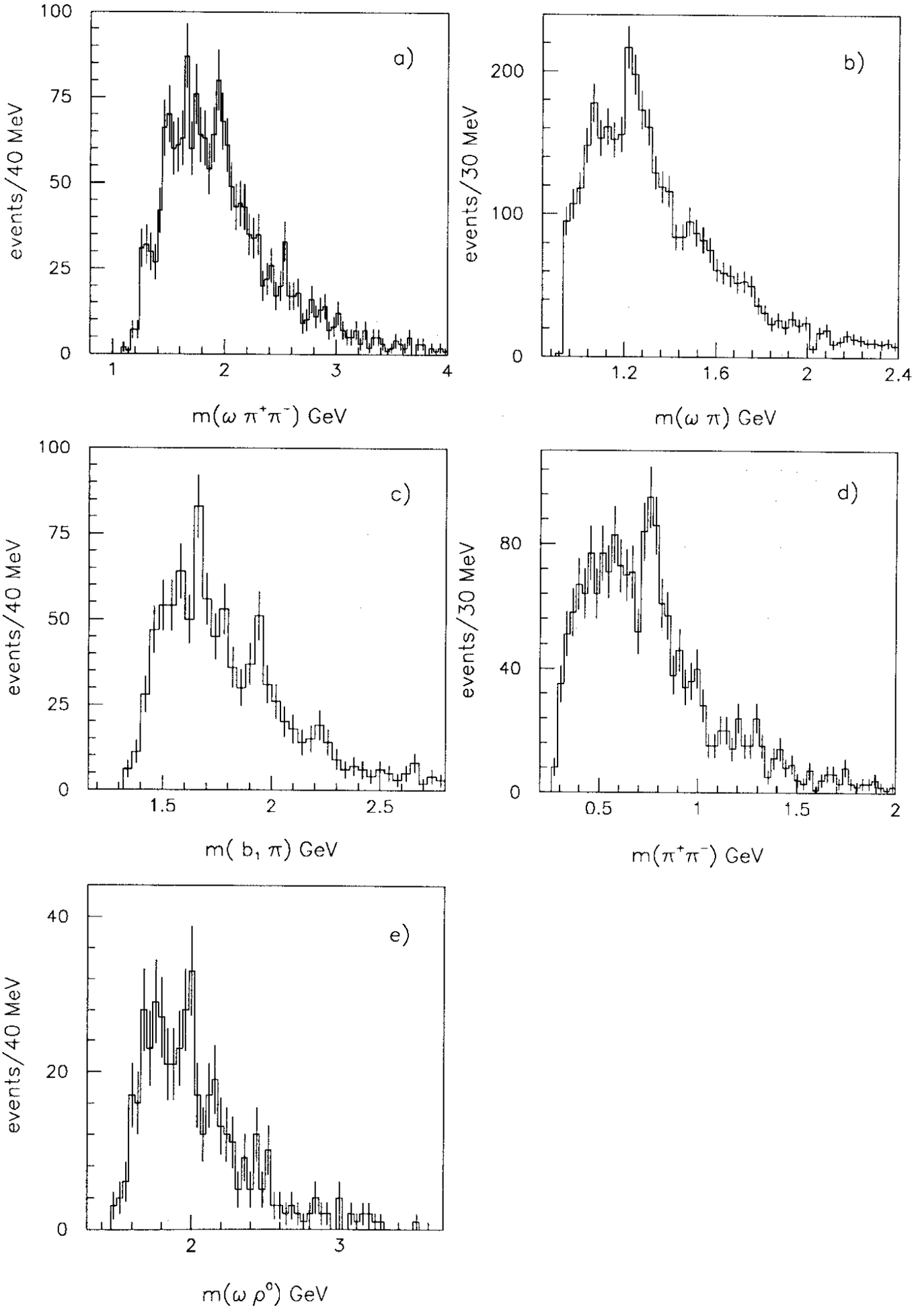
a)
b)
c)
d)
e)
events/40 MeV
events/30 MeV
m(ω π⁺π⁻) GeV
m(ω π) GeV
m(b₁ π) GeV
m(π⁺π⁻) GeV
m(ω ρ°) GeV

Fig. 6

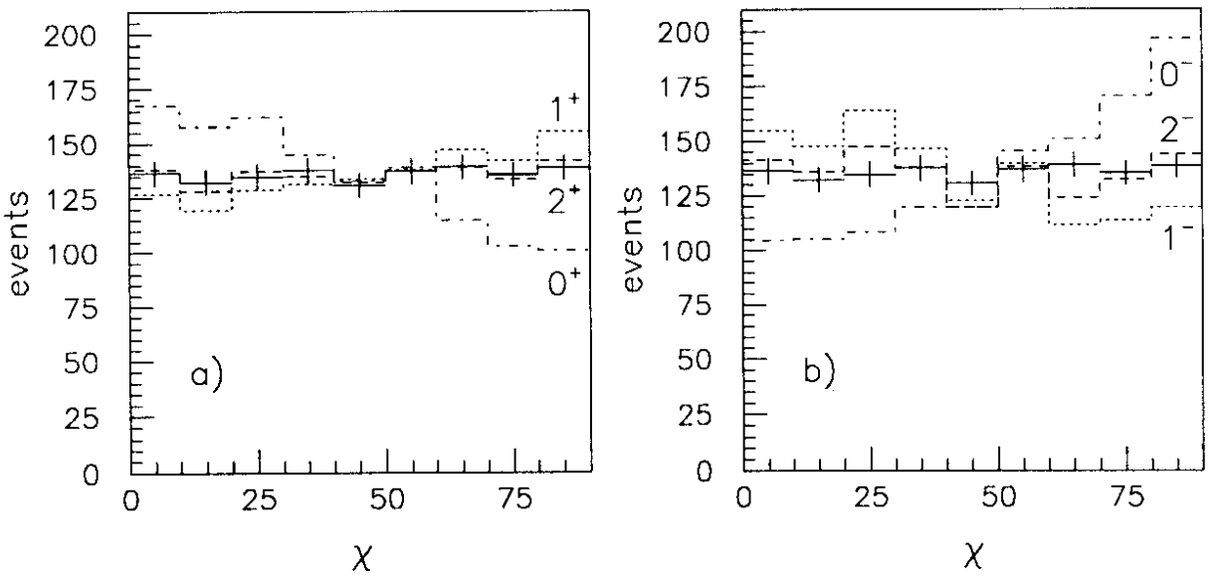
events
200
175
150
125
100
75
50
25
0
0
25
50
75
χ
1+
2+
0+
a)
events
200
175
150
125
100
75
50
25
0
0
25
50
75
χ
0-
2-
1-
b)

Fig. 7

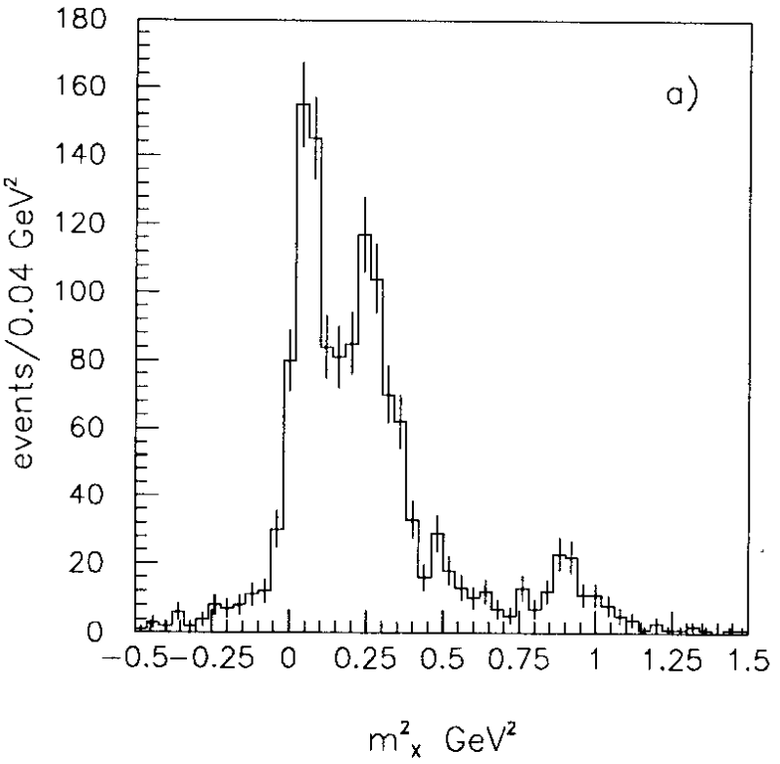
a)
events/0.04 GeV²
180
160
140
120
100
80
60
40
20
0
−0.5 −0.25 0 0.25 0.5 0.75 1 1.25 1.5
m²x GeV²

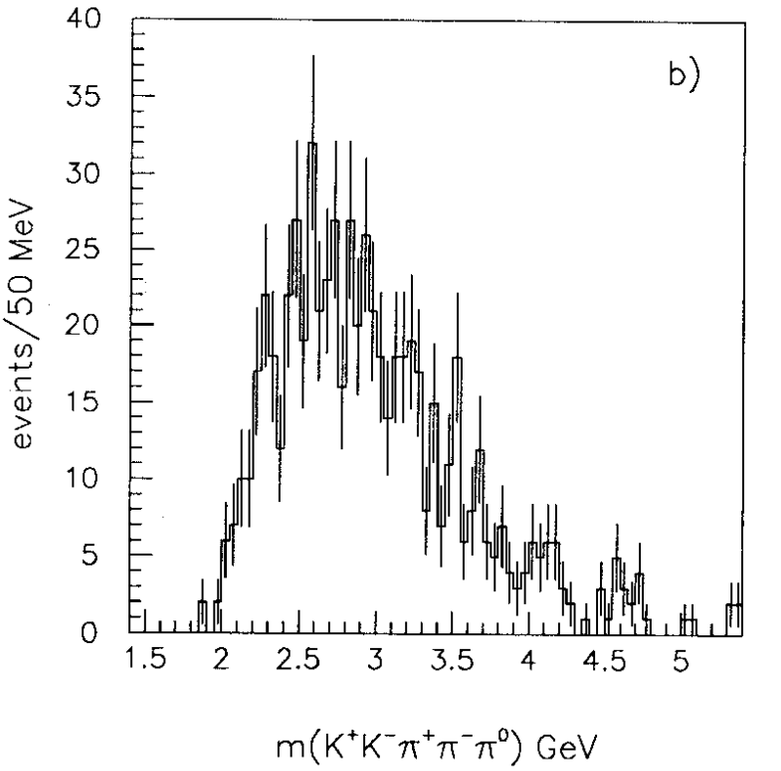
b)
events/50 MeV
40
35
30
25
20
15
10
5
0
1.5 2 2.5 3 3.5 4 4.5 5
m(K⁺K⁻π⁺π⁻π⁰) GeV

Fig. 8

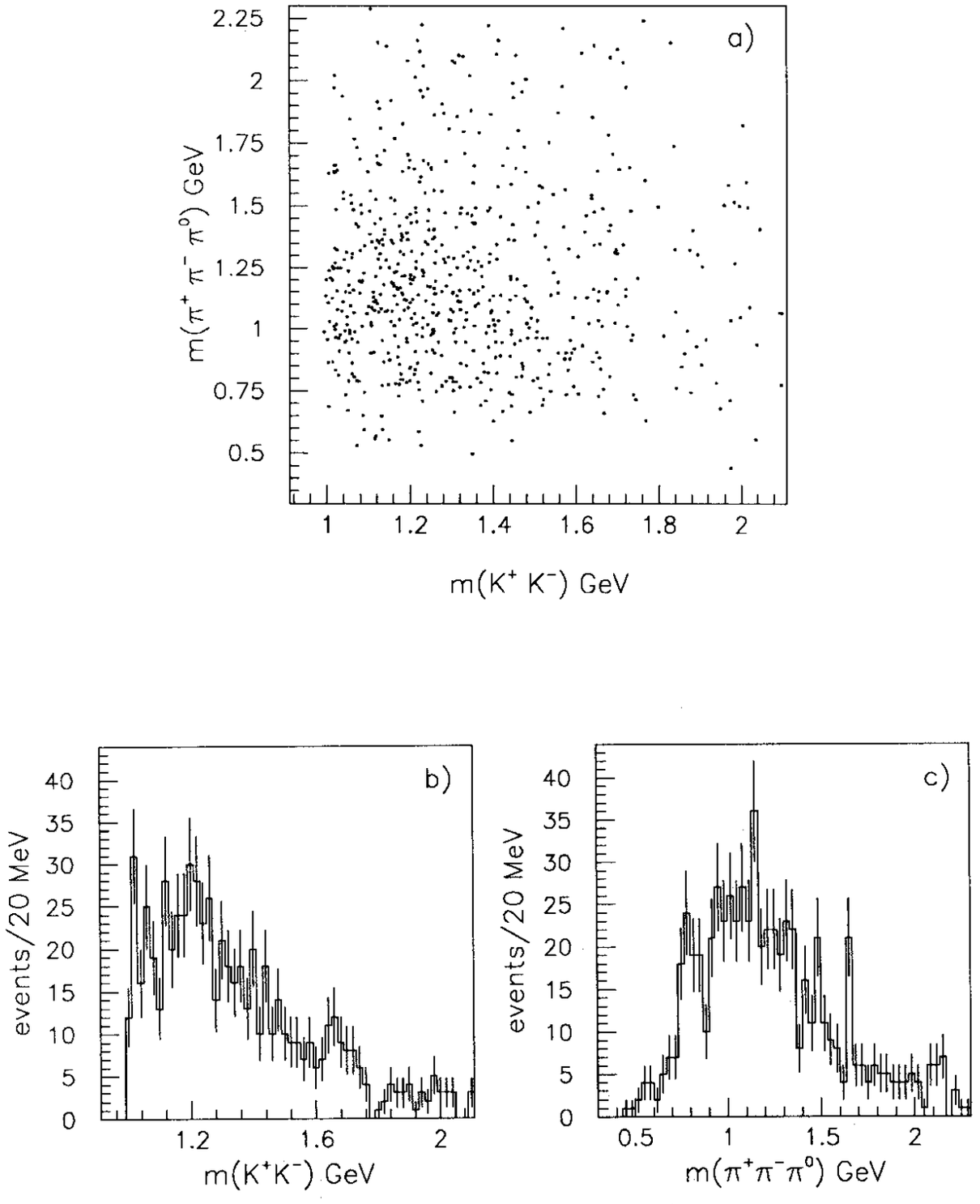
a)
2.25
2
1.75
1.5
1.25
1
0.75
0.5
m($\pi^+\pi^-\pi^0$) GeV
1
1.2
1.4
1.6
1.8
2
m(K^+K^-) GeV
b)
40
35
30
25
20
15
10
5
0
events/20 MeV
1.2
1.6
2
m(K^+K^-) GeV
c)
40
35
30
25
20
15
10
5
0
events/20 MeV
0.5
1
1.5
2
m($\pi^+\pi^-\pi^0$) GeV

Fig. 9

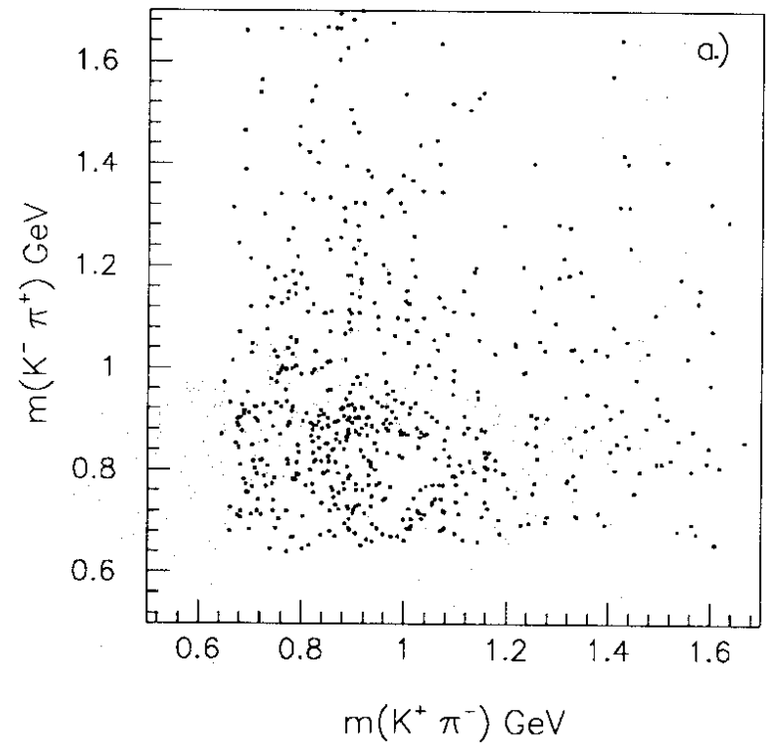
a.)
1.6
1.4
1.2
1
0.8
0.6
m(K⁻ π⁺) GeV
0.6
0.8
1
1.2
1.4
1.6
m(K⁺ π⁻) GeV

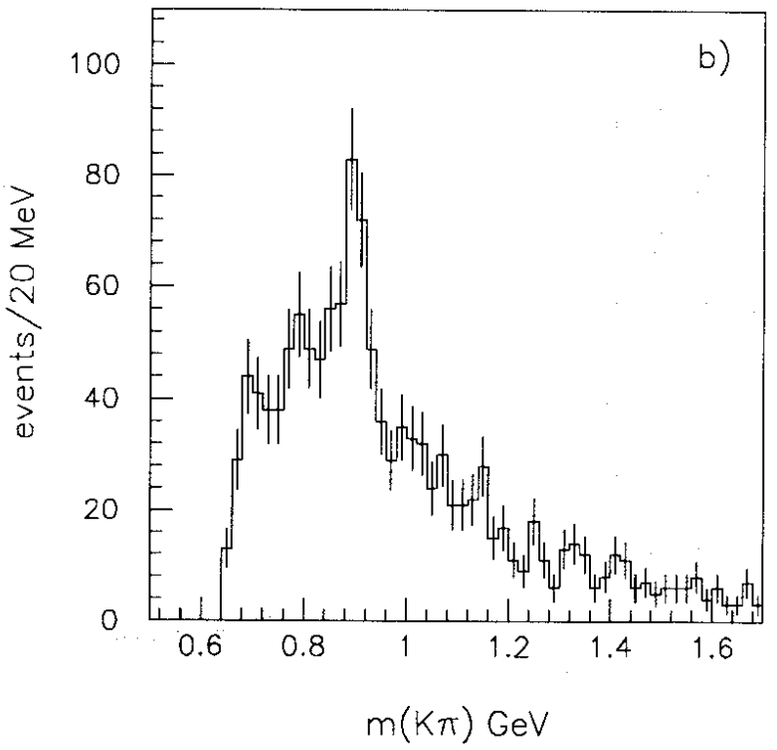
b)
100
80
60
40
20
0
events/20 MeV
0.6
0.8
1
1.2
1.4
1.6
m(Kπ) GeV

Fig. 10

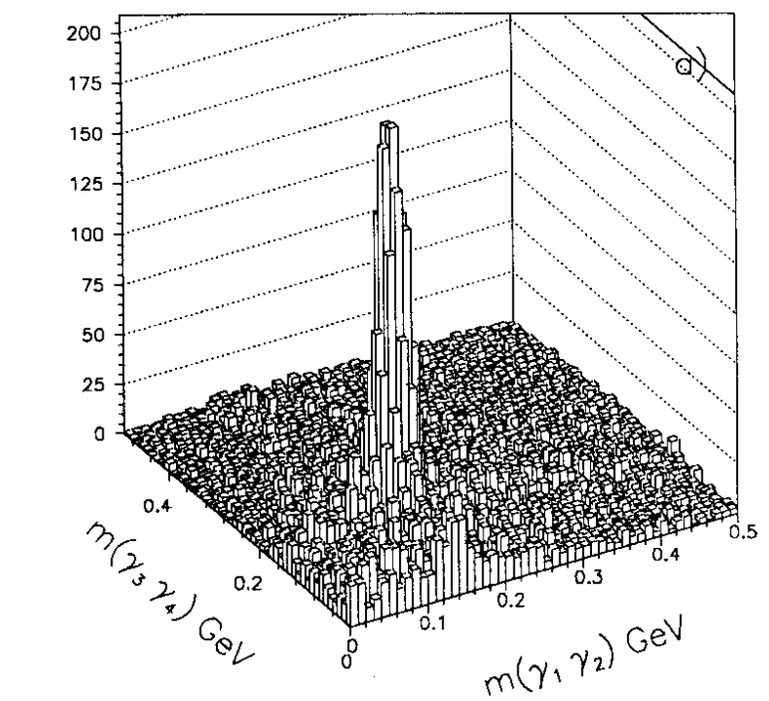
a)
200
175
150
125
100
75
50
25
0
0.4
0.2
0
$m(\gamma_3\gamma_4)$ GeV
0
0.1
0.2
0.3
0.4
0.5
$m(\gamma_1,\gamma_2)$ GeV

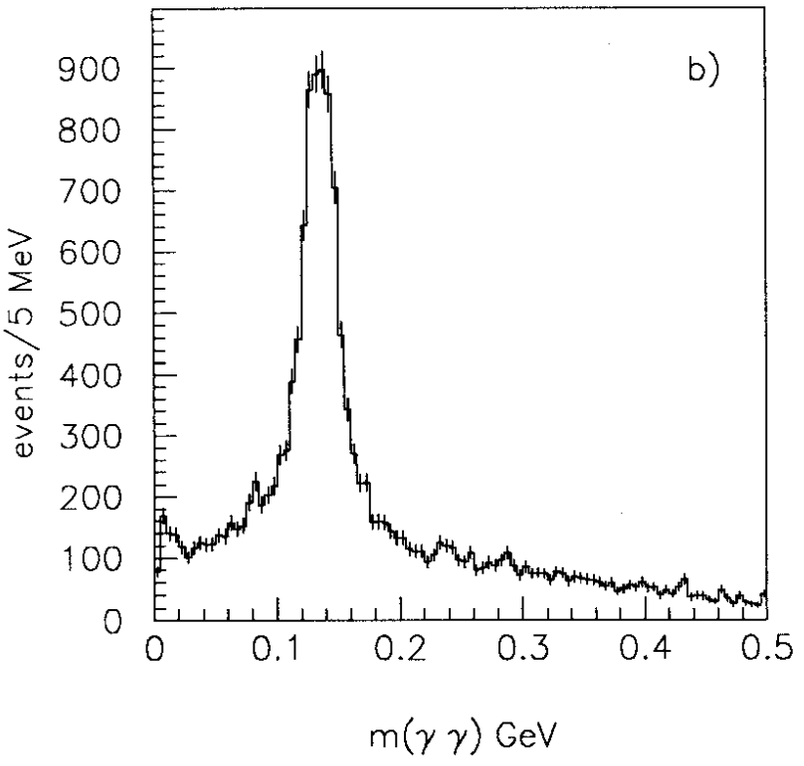
b)
900
800
700
600
500
400
300
200
100
0
events/5 MeV
0
0.1
0.2
0.3
0.4
0.5
$m(\gamma\ \gamma)$ GeV

Fig. 11

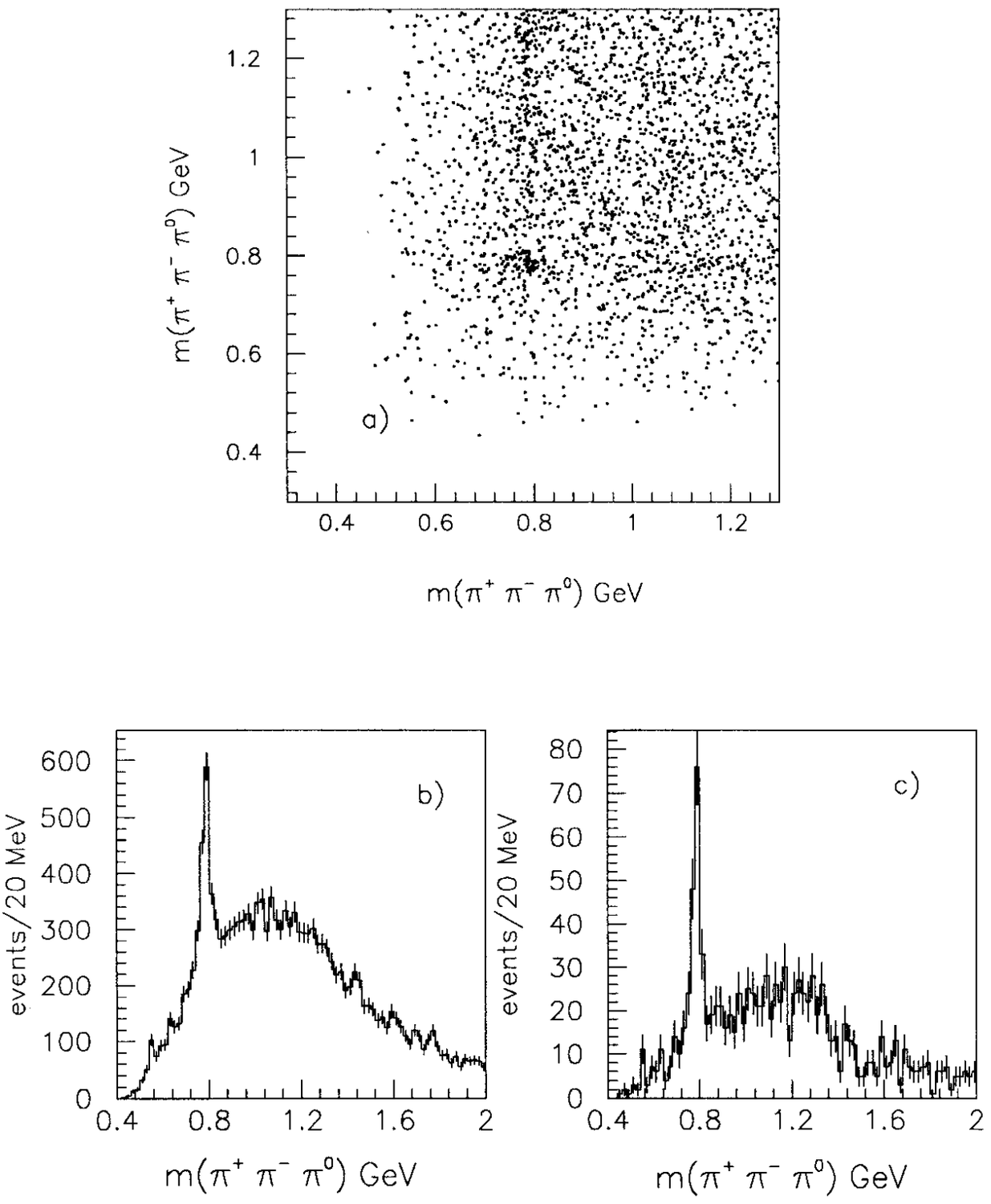

Fig. 12

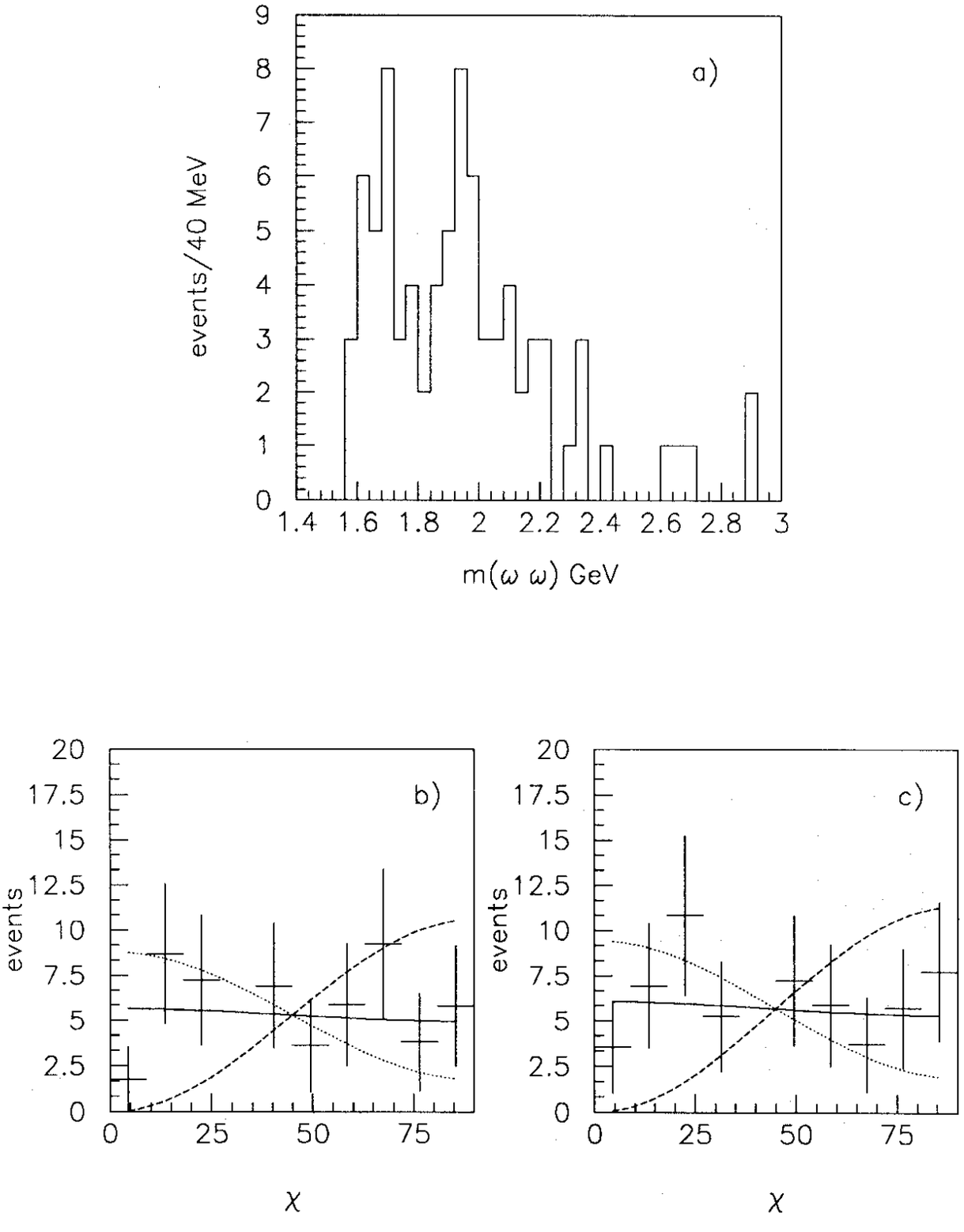

Fig. 13